Multiridge-Based Analysis for Separating Individual Modes From Multimodal Guided Wave Signals in Long Bones

ARTICLE *in* IEEE TRANSACTIONS ON ULTRASONICS, FERROELECTRICS, AND FREQUENCY CONTROL · NOVEMBER 2010

Impact Factor: 1.51 · DOI: 10.1109/TUFFC.2010.1714 · Source: PubMed

3 AUTHORS, INCLUDING:

Kailiang Xu
Pierre and Marie Curie University - Paris 6

Dean Ta
Fudan University

Multiridge-Based Analysis for Separating Individual Modes From Multimodal Guided Wave Signals in Long Bones

Kailiang Xu, Dean Ta, *Member, IEEE*, and Weiqi Wang

***Abstract*—Quantitative ultrasound has great potential for assessing human bone quality. Considered as an elastic waveguide, long bone supports propagation of several guided modes, most of which carry useful information, individually, on different aspects of long bone properties. Therefore, precise knowledge of the behavior of each mode, such as velocity, attenuation, and amplitude, is important for bone quality assessment. However, because of the complicated characteristics of the guided waves, including dispersion and mode conversion, the measured signal often contains multiple wave modes, which yields the problem of mode separation. In this paper, some novel signal processing approaches were introduced to solve this problem. First, a crazy-climber algorithm was used to separate time-frequency ridges of individual modes from time-frequency representations (TFR) of multimodal signals. Next, corresponding time domain signals representing individual modes were reconstructed from the TFR ridges. It was found that the separated TFR ridges were in agreement with the theoretical dispersion, and the reconstructed signals were highly representative of the individual guided modes as well. The validations of this study were analyzed by simulated multimodal signals, with or without noise, and by *in vitro* experiments. Results of this study suggest that the ridge detection and individual reconstruction method are suitable for separating individual modes from multimodal signals. Such a method can improve the analysis of skeletal guided wave signals by providing accurate assessment of mode-specific ultrasonic parameters, such as group velocity, and indicate different bone quality properties.**

I. Introduction

Osteoporosis, which increases the risk of bone fracturing, has become prevalent worldwide because of the aging population [1]–[3]. Many useful methods have been established for diagnosing this disease, including quantitative CT (QCT), dual-energy X-ray attenuation (DXA), and three-dimensional X-ray bone densitometry [3]–[5]. Although DXA still is the clinical standard for diagnosing osteoporosis, this approach has some disadvantages such as radioactivity, bulky instruments, and relatively high cost. Most importantly, DXA does not accurately identify individuals who will later sustain a fracture [6], [7]. Quantitative ultrasound (QUS) offers significant advantages over these X-ray based methods, as it does not include ionizing radiation and ultrasonic devices can be made inexpensive and portable. Furthermore, QUS is highly sensitive to both geometric and material properties of the bone. Specifically, ultrasonic guided waves provide a viable QUS approach for the assessment of long cortical bones [2], [5], [8]–[10].

Ultrasound velocity measurement in long bones is typically based on axial transmission approach. The measurement configuration consists of two transducers placed along the axial direction of the pipe-shaped long bone, and the incidence angle and transmission distance can be tuned and optimized for any wave mode of interest [2], [8], [10]. Although the axial transmission approach is based on a simple setup, the received guided wave signals are complicated. The signal tends to spread because of dispersion and interferences between multiple propagating wave packets which correspond to individual guided modes. As a result, it is often very challenging to separate these individual modes. Time-frequency representation (TFR) is a commonly used method for analyzing such multimode signals, because it provides a clear illustration for the temporal variation modal energy stream in the time-frequency domain. Short-time Fourier transform (STFT) is the simplest TFR approach available, and it has been used to identify modes L(0,2) and L(0,3) from a series of bovine tibia signals [11]. Recently, some improved TFR methods, such as reassigned spectrogram, smoothed-pseudo Wigner-Ville and its reassigned version, have been used to analyze the dispersion properties of guided modes, and detailed comparisons between the theoretical dispersion curves and the TFR energy distributions have been carried out [10], [12]. These studies already investigated some multimodal signals, but did not report proper modes extraction of quantitative data [10]–[14]. If some advanced separation algorithms can be adopted in the TFR analysis of multimodal signals, accurate quantitative data on propagation characteristics of individual modes, such as energy [12], arriving time, attenuation [14], amplitude, and transmission and reflection coefficients [15] can be obtained, which further reflect different properties of the bone as a waveguide. Such accurate information on propagation characteristics of individual modes can essentially enable inverse assessment of individual bone properties from ultrasonic signals. There is a call for such methods of signal processing, because those methods can highly improve multimodal bone assessment. Nevertheless, an efficient separation of guided modes remains a challenging task for signal processing [8].

Manuscript received January 12, 2010; accepted July 15, 2010. This work was supported by the National Natural Science Foundation of China (No.10774029, 30870720), the Ph.D. Programs Foundation of the Ministry of Education of China (No. 20090071110066), and the Shanghai Leading Academic Discipline Project (No. B112).

The authors are with the Department of Electronic Engineering, Fudan University, Shanghai, P.R. China (e-mail: tda@fudan.edu.cn).

Digital Object Identifier 10.1109/TUFFC.2010.1714

Studies attempting to address this problem could be divided into two main categories, selective mode excitation and modes separation. In case of selective mode excitation, a transducer array with a multichannel time-delay system has been applied to improving mode control and selection [16]. Magnetostrictive sensors were suggested to excite axisymmetric modes in industrial pipes [17]. However, the anatomical geometry of the human long bone is irregular, thus there has been little progress in implementation of the selective excitation, especially at a low frequency. As for modes separation, two-dimensional fast Fourier transform (2-D-FFT) has been widely used to obtain some individual modes from a group of multimodal signals [18]. Moilanen *et al.* [19] used group velocity filtering (a kind of time domain mask window) to selectively envelop a region of interest from the measured distance-time signal diagram. After that, the resolution of the 2-D-FFT was improved, and an inversion scheme to determine the plate thickness was further discussed. However, for all of the 2-D-FFT based methods, several signals recorded within a finite source-receiver distance are needed to achieve a sufficient spatial resolution. This kind of shift technique (i.e., analysis of a series of signals recorded within a range of source-receiver distance) inherently assumes that long bones have a uniform shape, which is somewhat unrealistic. The variation of bone material properties and geometry within this region of interest may critically affect the propagation characteristics of certain guided modes. This may cause inconsistency in the modal contents of the spatial signal, and the 2-D-FFT cannot then provide unambiguous mode identification. Also, it is difficult to separate the time-domain waveform of the individual mode components from multimodal signals by the 2-D-FFT method. Thus, other interesting and useful methods have been proposed. Niethammer *et al.* [20] introduced the empirical mode decomposition (EMD) method into ultrasonic nondestructive evaluation (NDE), which is a crucial step of the Hilbert-Huang transform (HHT) [21], but they failed to separate the individual modes during the analysis of multiple modes. Later, Luo *et al.* combined the HHT with wavelet packet decompositions to reduce the noise and mutual disturbance among different modes, and estimated bovine cortical thickness [22]. Recently, a singular value decomposition-based algorithm, taking the benefit of multi-receiver array signal, was also applied to extract the most energetic late arrival contribution, whose velocity was shown to be highly correlated to cortical bone thickness [23]–[25].

In this paper, being attracted by the fact that the guided modes can be identified in TFR [11], [26]–[28], we used an interesting crazy-climber time-frequency ridge detection method [29] to separate TFR ridges corresponding to individual wave modes, and then applied the TFR ridge penalization algorithm to reconstruct corresponding waveforms in the time domain. The whole process can be accomplished without any *a priori* knowledge, which is an advantage of the method.

The paper is organized as follows. In Section II, detailed introductions for the TFR, separation, and reconstruction method are provided. Basic theory of the waveguide and methods of simulations are illustrated in Sections III-A and III-B, and *in vitro* experiments on bovine tibiae are described in Section III-C. Results of separation and reconstruction are shown in Section IV. The simulations are analyzed under different levels of added synthetic noise. The extracted individual modal components are also compared with the theoretical results in this section. Conclusions will be given in the last section.

II. Multiridge Detection and Reconstruction Method

Many time-frequency methods have been applied to ultrasonic NDE because of the capability of these techniques to represent the time-varying components of the guided waves [12], [20]. Recently, De Marchi *et al.* implemented a warped frequency transform, which can fit the time-frequency plane to the dispersion curve of certain mode, and therefore enhance its TFR resolution and extraction capabilities [30], [31]. Apparently, different TFR methods, including time-frequency [32] and time-scale (wavelet) transforms [33], have different properties, but their common idea is to characterize the temporal frequency of the time-varying signals. For convenience, TFR will be restricted to the STFT hereinafter.

The separation work was first proposed by McAulay and Quatieri for speech analysis/synthesis [34]. They built a sinusoidal model that can estimate the temporal phase, frequency, and amplitude for speech reconstructions. This model can also be used to separate components of a multimodal signal because the temporal parameters are easier to divide than the TFR energy distribution. Later, Carmona *et al.* [29] developed a systemic separation and reconstruction method based on the TFR ridges, which can mark the energy-concentrated region of the time-frequency plane. It is capable of handling the compression and reconstruction of multiple components in speech signals. This paper applied the algorithm to multimode separation. As Fig. 1 shows, first, the TFR of the input signal is obtained by STFT. Second, the temporal frequencies of the guided modes with corresponding amplitude (e.g., TFR ridges) can be achieved by the crazy-climber algorithm. Third, the individual components are obtained by reconstruction method. Because a singular mode is subject to being separated into pieces of ridges, the reconstructed waveform pieces need to be selectively added together in the end.

This section is arranged as follows. Part A explains one of the basic TFR methods, STFT. Part B introduces the TFR multiridge detection and separation algorithm (called the crazy-climber method [29]). The individual TFR ridge-based mode reconstruction procedure will be described in part C.

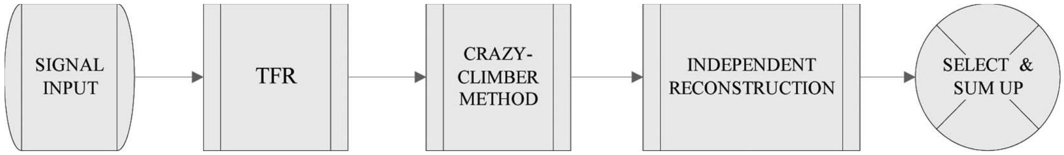

Fig. 1. Block diagram of the TFR multiridge detection and component reconstruction.

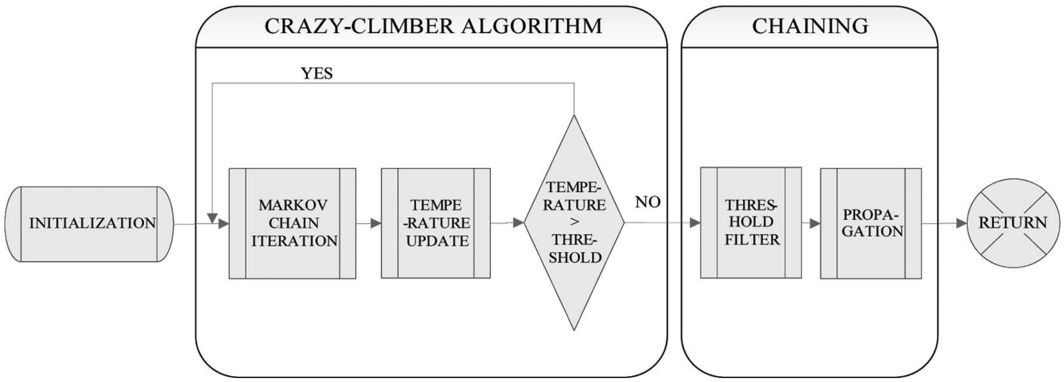

Fig. 2. Block diagram of the multiridge detection and separation algorithm.

A. Short Time Fourier Transform (STFT)

To meet the requirement of non-stationary signals, a large number of TFRs have been developed. By taking the spectra of a series of signal pieces divided by short overlapping windows, we can observe how the energy distribution of a signal varies with time. This is the essential idea of the STFT, which is defined for a signal $s(t)$ as [32]

$$\mathrm{TFR}_{\mathrm{STFT}[s(t)]}(u,v) = \frac{1}{2\pi}\int_{-\infty}^{\infty} e^{-jvt} s(t) h(t-u)\mathrm{d}t, \qquad (1)$$

where $h(t)$ is a short time window, and consequently the time-frequency atom can be defined as $\varphi_{u,v}(t) = e^{iv(t-u)}h(t - u)$. The energy density spectrum of the STFT is simply called spectrogram and given by $E(u,v) = |\mathrm{TFR}_{\mathrm{STFT}}(u,v)|^2$. The resolution limitation between time and frequency is the so-called time-frequency tradeoff, which has been concluded by an uncertainty principle, e.g., Gabor-Heisenberg inequality [32]. To offset the uncertainty and some the cross-terms [32] in TFR, some modified time-frequency methods have been proposed. Traditionally speaking, they can be mainly divided into two categories: Cohen's-class bilinear time-frequency distributions [32] and affine-class time-frequency distributions [35]. For the applications of waveguides, all of these methods are able to reflect the time-frequency properties of the energetic guided components [12]. Because many parameters of guided waves can be computed theoretically (as described in Section III-A), TFRs provide means for estimating the characteristics of the waveguide inversely. Recently, many studies on guided waves were done by comparing TFRs with the theoretical dispersion curves. However, if the TFR ridges can be separated, and the associated mode components can be further reconstructed, the parameters of the existing modes, for example, velocity, attenuation, transmission, and reflection coefficients, can be analyzed individually. This is the fundamental goal of multiridge-based analysis of modes separation and reconstruction, and it is a valuable topic of waveguide signal processing.

B. TFR Multiridge Detection and Separation Algorithm

TFR multiridge detection and separation method is based on the Markov chain Monte Carlo approach [36]. The crazy climbers are able to determine all local maxima rather than global maxima. Afterward, a chaining trick is used to obtain the individual TFR ridges (also called skeletons). Fig. 2 shows the block diagram of the multiridge detection and separation algorithm.

The real signal is always a non-analytic signal with a TFR that contains negative frequencies. However, we can focus on the upper half of the time-frequency plane (T, F) in the domain $D = (T > 0,\ F > 0)$ because the negative and positive frequencies are mutually mirrored. TFR in D is denoted as $m(T, F)$, and its modulus is given by $|m(T, F)|$. For implementation, we discretized the domain D as $T = \{0, \ldots, T_{L-1}\}$ and $F = \{0, \ldots, F_{M-1}\}$. Then the modulus TFR becomes an $L \times M$ matrix.

1) Crazy-Climber Algorithm:

1) Initialization: At time $t_0 = 0$, the position set of the climbers $X(t_0) = \{(j, k);\ j = 0, \ldots, T_{L-1};\ k = 0, \ldots, T_{L-1}\}$ are randomly initialized with a uniform probability distribution in the domain D and the temperature is set to temp_0.
2) Markov chain iteration: Because each crazy climber is independent of the others, it will not reduce generality to discuss the statistical property of a single climber. Assuming that at time t, the position is $X(t) = (j, k)$, at time $t + 1$, the position $X(t + 1) = (j', k')$ will be arranged in two steps. The first one is the horizontal adjustment. If $1 \le j \le T_{L-1} - 1$, then the

climber can move to the right or left with the same probability, $P\{j' = j+1\} = P\{j' = j-1\} = 1/2$. The second step is the vertical adjustment: up ($k' = k + 1$) or down ($k' = k - 1$). If $|m(j', k')| > |(j', k)|$, then $X(t+1) = (j', k')$. If $|m(j', k')| < |(j', k)|$, the climber will move depending on the probability to $X(t+1) = (j', k')$ with $P_t = \exp\{[|m(j', k')| - |m(j', k)|]/\text{temp}_t\}$ and to $X(t+1) = (j', k)$ with $1 - P_t$. After moving, the temperature temp_t must be adjusted to 0 step by step. It has been proven that $\text{temp}_t = \text{temp}_0/\log_2 t$ ensures that the system can converge to a global minimum.

3) Iteration ending: The iteration will be ended when the temperature is lower than a certain threshold.

2) Chaining:

In the beginning, the positioned climbers, as the output of the crazy-climber process, are filtered by a threshold which is used to distinguish the climbers lost in the pseudo peaks. Some random noise, reflections, and scatters can be removed by this step. Then, for the remaining climbers on each ridge, an iterative trick is used to chain the fittest neighbors one by one.

C. Individual Modes Reconstruction From the TFR Ridges

When the TFR ridges are detected by the crazy-climber algorithm, their temporal frequencies can be used to create the reconstruction constraints because the TFRs components of the estimated $\hat{s}(t)$ must take the same value on each sample point of the abstracted ridges. Furthermore, $\hat{s}(t)$ cannot oscillate too widely, either. This problem can be formulated as a solution of minimization [29]

$$\hat{S} = \arg\min_f \left\{ \frac{1}{n} \left\| \Sigma^{-1/2} \left[\mathrm{TFR}_{\mathrm{s}} - \mathrm{TFR}_f \right] \right\|^2 + \eta \langle Qf, f \rangle \right\}, \tag{2}$$

where $||\cdot||$ denotes the Euclidian norm. The first term, called the Mahalanobis distance, is a weighted sum of the squares, where the weights are defined by the inverse of the covariance matrix. If the covariance matrix is the identity matrix, the Mahalanobis distance reduces to the Euclidean distance. Here, it is used to ensure that the TFR of the estimation TFR_f is identical to TFR of the original signal ($\mathrm{TFR}_{\mathrm{s}}$) on each sample point of the ridge. The second term is a penalty term to prevent $\hat{S}$ from oscillating too widely, and the reconstruction kernel Q is defined by [29]

$$\begin{aligned} Q(x,y) = \delta(x-y) + \varepsilon \sum_i \Big\{ \int \Big(& g'(x-u) g'(y-u) \\ & + g(x-u) g(y-u) \cdot [(x-u)(y-u) v_i'(u)^2 \\ & - (x+y-2u) v_i(u) v_i''(u)] \Big) \cdot \cos(v_i'(u)(x-y) \mathrm{d}u \\ & + \int \Big(g'(x-u) g(y-u) [v_i(u) - (y-u) v_i'(u)] \\ & \cdot g(x-u) g'(y-u) \cdot [v_i(u) - (x-u) v_i'(u)] \Big) \\ & \cdot \sin(v_i(u)(x-y)) \mathrm{d}u \Big\}, \end{aligned} \tag{3}$$

where i denotes the number of the ridges detected from the TFR. The solution of this minimization problem can be written as

$$\hat{S}(t) = \sum_i \sum_{j=1}^{2n_i} \lambda_{i,j} Q^{-1} \varphi_{i,j}(t), \tag{4}$$

where $\varphi_{i,j}(t)$ is the time-frequency atom (see definition in Section II-A) at the jth sample point of the ith ridge, and $2n_i$ denotes the number of real constraints from the n_i complex constraints of the TFR consistency between the estimated and original signals. The $\lambda_{i,j}$ can be computed from $2n_i$ linear equations by Lagrange multipliers method, and consequently the estimated $\hat{S}(t)$ can be calculated from (4).

III. Simulations and Experiments

A. Guided Wave Theory

A hollow cylinder filled with the viscous liquid was used to model the guided wave propagation in the elastic long bone. The mechanical properties of cortical bone were considered to be isotropic and homogeneous. The outer boundary of the cortical bone was considered traction free. Bone marrow was assumed to be a viscous Newtonian liquid obeying the linearized Navier-Stokes equation [14], [37]. Therefore, the axial and radial displacements are continuous, and the radial stress in the inner surface of cortical bone is equal to the pressure in the marrow. According to the elastic dynamic motion equation and boundary conditions, the characteristic equation is written [14]

$$[M_{ij}] \cdot [N] = 0, \quad i, j = 1, 2, \ldots, 6, \tag{5}$$

where $N = [A\ B\ A_1\ B_1\ A_m\ B_m]^T$ and A, B, A_1, B_1, A_m, and B_m are unknown amplitudes. M_{ij} is a coefficient matrix [14]. To obtain a non-trivial solution of this model, the determinant of the coefficient matrix should be zero [14]:

$$\left| M_{ij} \right| = 0. \tag{6}$$

Eq. (6) is the dispersion equation of the guided waves in the long bone, which can be used to calculate the dispersion curves for generating the simulated signals and comparing with the mutimodal TFRs.

B. Simulations

The proposed signal processing method was tested on synthesized multimodal guided wave signals. Let $u(x,t)$ denote the out-of-plane surface displacements of the mode of interest in the model, where the x is the axial propagation distance, e.g., distance between the axial transducers, and the t is the time, the corresponding waveform of this mode can be calculated by [38]

$$u(x,t) = \int_{-\infty}^{+\infty} F(\omega) e^{i(k(\omega)x - \omega t)} \mathrm{d}\omega, \tag{7}$$

where $k(\omega)$ is the wavenumber dispersion curve of the mode of interest as a function of frequency; $F(\omega)$ is the spectrum of the input signal, e.g., the excited impulse; and here, a Gaussian-envelope signal was used. The theoretical dispersion curve of each mode can be calculated by the pipe-shaped model that we discussed previously. The multimodal synthetic signal is the sum of several individual simulated modes. Thus, the amplitude of each individual mode can be arbitrarily decided, which is helpful for the comparison between the simulation and separation results. Acoustic properties of cortical bone were modeled by the density $\rho = 1.90$ g/cm^3, compression wave velocity $C_l = 4.00$ m/ms, and shear wave velocity of $C_t = 1.97$ m/ms [14]. The wall thickness was 5.5 mm and inner radius of curvature 21.5 mm, based on X-ray CT on bovine tibia specimens used in the study.

C. Experimental Setup and Bone Samples

The experimental setup for *in vitro* ultrasonic guided wave measurements in long bones is shown in [14]. The pulser/receiver unit 5900PR (Panametrics Corp., Waltham, MA) was used to excite the transducer and to receive signals. Two different transducers were used in our experiment; both had center frequencies of 0.5 MHz (bandwidth 0.2 to 0.8 MHz). The transmitter was a vertical transducer; the receiver was an oblique transducer with a 45° angle. The vertical transmitter was fixed, and the oblique receiver can incrementally move along the axial direction of the long bone. Movement in the axial direction was controlled by UltraPAC step motors (Physical Acoustics Corp., Princeton Junction, NJ). The guided waves at different sites on the bone can be measured. All measurements were performed at temperature of 22°C. Ultrasonic gel (Echo Jelly; Aloka Medical Equipment Co., Shanghai, China) was used as a coupling agent to guarantee that the transducers were compacted to the bone surface. The influence of the gel on the signals was ignored. The received signals were averaged 256 times, amplified, and digitized to 8 bits (HP54642A; Hewlett-Packard, Palo Alto, CA) at a speed of 20 mega-samples per second.

It should be noted that modes L(0,2), L(0,3), and L(0,4) have already been observed and identified in such bovine bones in our earlier study [14], where the same experimental setup was used. In the present paper, modes L(0,3), L(0,4), and L(0,5) were observed, and the synthetic test signals were composed correspondingly. Nevertheless, the purpose of the study was to evaluate the mode separation ability of the proposed method on such signals, without specifically taking a stance on any experimental setup or exact modal contents of the response.

IV. Results and Discussion

For a certain long bone model, after calculating its dispersion curves by (6), the time-domain waveforms were synthesized by (7). Longitudinal tube modes L(0,m), $m = 3$, 4, and 5, were superimposed in these simulated signals, consistently with modes observed on *in vitro* test experiments. Our earlier *in vitro* axial transmission studies have already reported on observation and identification of these higher-order L(0,m) modes in bone [11], [14]. In these studies, frequency-to-thickness products of around 1 to 3 MHz·mm and oblique incidence and/or reception were used, as in the present study. On the other hand, several other studies using lower frequency-to-thickness products of around 0.1 to 1.0 MHz·mm have reported on observation and identification of the fundamental flexural mode F(1,1) (also referred as A0 by some studies) in bone [39]–[41]. Composition of a multimodal signal is thus determined by the experimental setup used. The methods presented here can be applicable to any multimode signal composition.

A. Simulated Signals Without Noise

We begin with presenting the waveform of mode L(0,3) [see Fig. 3(a)] as an example. The multimode waveform is computed by the sum of the L(0,3), L(0,4), and L(0,5) [see Fig. 3(c)]. Considering the length of simulated signals is 1250 points, a 301-point Gaussian window function, about a quarter of the signal length, was used to calculate the TFRs by the STFT. The TFR of the multimodal signal is depicted in Fig. 3(c) with its TFR ridges obtained by crazy-climber algorithm (500 climbers) in Fig. 3(d), where the color of the ridges (in the online version of the figure) denotes the energy intensity on the sample points of the TFR. Dispersion curves of L(0,3), L(0,4), and L(0,5) are plotted on the time-frequency plane for comparison. As expected, the multimodal TFR ridges focus on the time-frequency regions in which the signal energies are concentrated [see Fig. 3(d)]. In addition, it is shown that the three modes can be separated by three ridges. However, there seems to be some discrepancy between the ridges and the dispersion curves, which are implied by the time-frequency uncertainty principle, e.g., the time and frequency position information of each time-frequency atom cannot be determined accurately and simultaneously. The energy of each time-frequency atom easily leaks to the adjacent time-frequency grids, and both are to be covered by the TFR ridges. Each of the ridges can be used to reconstruct the corresponding original components.

The idea of the proposed method is to reconstruct the original components from the separated ridges which are obtained from the multimodal TFR. Thus, it will never distinguish the reconstructed and the separated signal hereafter. An example of the reconstructed component L(0,3) is exhibited in Fig. 4(a), with its TFR in Fig. 4(b). Although the ridges are not accurate because of time-frequency uncertainty, both the waveform and TFR of the reconstructed L(0,3) are in agreement with the original one [Figs. 3(a) and 3(c)]. The total signal, which is the sum of three modes independently reconstructed, is given in Figs. 4(c) and 4(d). Comparing Fig. 4(c) and Fig. 3(b), there is almost no difference between the reconstructed and original signals, except that the early 50-μs amplitude

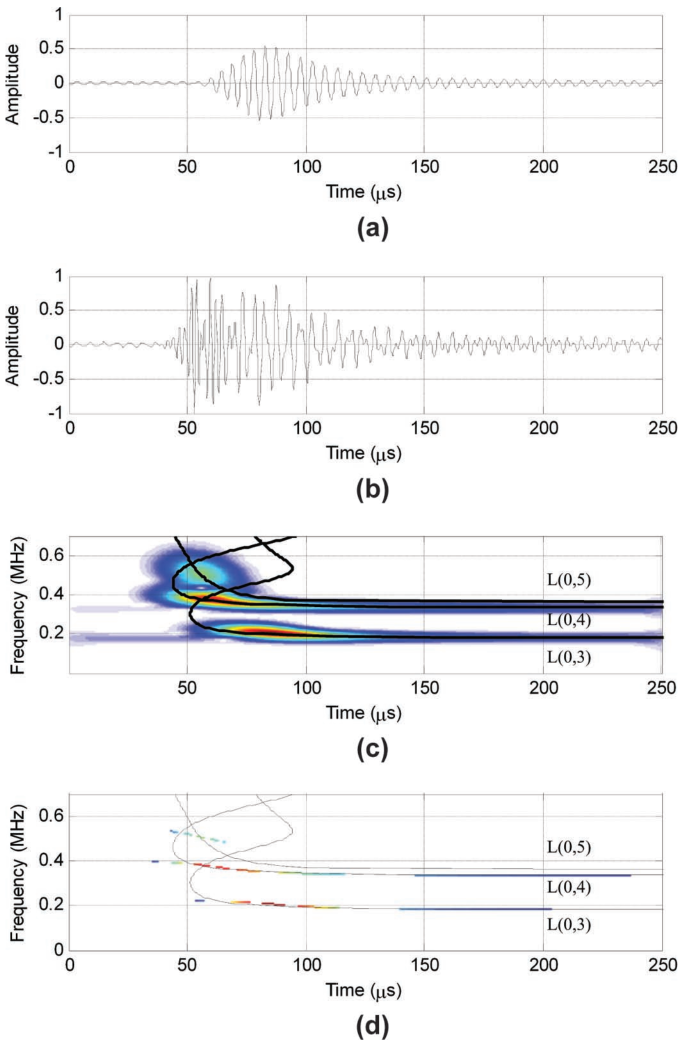

Fig. 3. Original noise-free simulated signals: (a) waveform of mode L(0,3), (b) waveform, (c) time-frequency representation (TFR) and (d) TFR ridges of the multimodal signal containing the L(0,3), L(0,4), and L(0,5) modes.

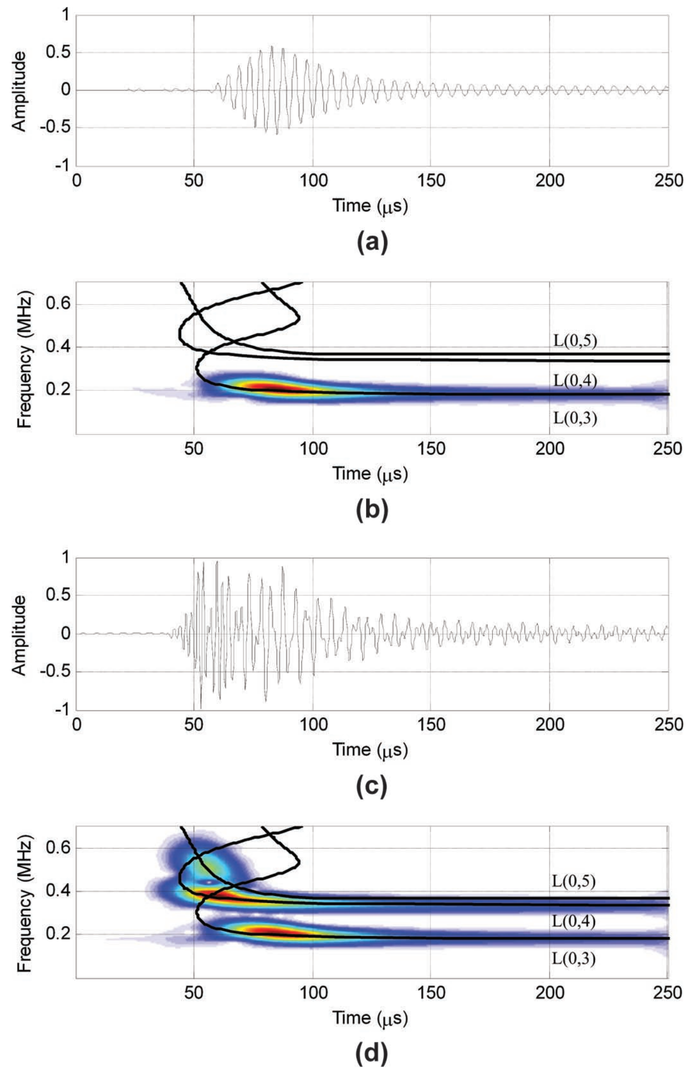

Fig. 4. Separated and reconstructed results of the noise-free simulated signal: (a) waveform and (b) TFR of the separated component L(0,3), (c) waveform and (d) TFR of the reconstructed multimodal signal (the sum of all the individually separated components).

of the reconstructed signal seems to be less than that of the original one. Because the early 50-μs TFR, with small modulus values of TFR, are considered to be some noise, it is removed by the threshold filter of the ridge chaining step. The normalized root mean square error (NRMSE) of the total reconstruction is about 1.38% and the NRMSE of L(0,3), L(0,4), and L(0,5) are about 0.82%, 1.53%, and 2.45%, respectively [see Fig. 7(a), ($\mathrm{SNR} = \infty$)]. More quantitative evaluations of the reconstruction will be discussed later.

B. Simulated Signals With Noise

To test the robustness of the proposed method, some white Gaussian noise was added into the signal (SNRs from 0 to 15 dB). The results of the separation under the SNR = 0 dB condition can be seen in Figs. 5 and 6. Fig. 5(a) shows the noisy simulated waveform, where the SNR is 0 dB. It is difficult to recognize the original signal in such a high-noise situation. Fortunately, an overview of the multimodal energy distribution can be identified from the TFR of the noisy signal in Fig. 5(b). The TFR ridges displayed in Fig. 5(c) are not strongly impacted by the noise and the TFR energy of each mode is successfully tracked and separated by the ridges. The reconstructed component L(0,3) and its TFR are shown in Figs. 6(a) and 6(b). The reconstructed result of Fig. 5(a) is shown in Fig. 6(c) with TFR in Fig. 6(d). Comparing Fig. 3(b) with Fig. 6(c), the reconstructed components from the noisy signals retain most of their energies as well. It is also found that the maximal amplitude of reconstructed L(0,3) is identical to the original waveform [see Figs. 3(a), 4(a), and 6(a)], which indicates that during the reconstruction, the component ratios of different modes are kept invariant. It indicates that the separation method can be applied to calculating the energy ratio [10], attenuation [12], reflection, and transmission coefficients [13] for each mode in the multimodal signal.

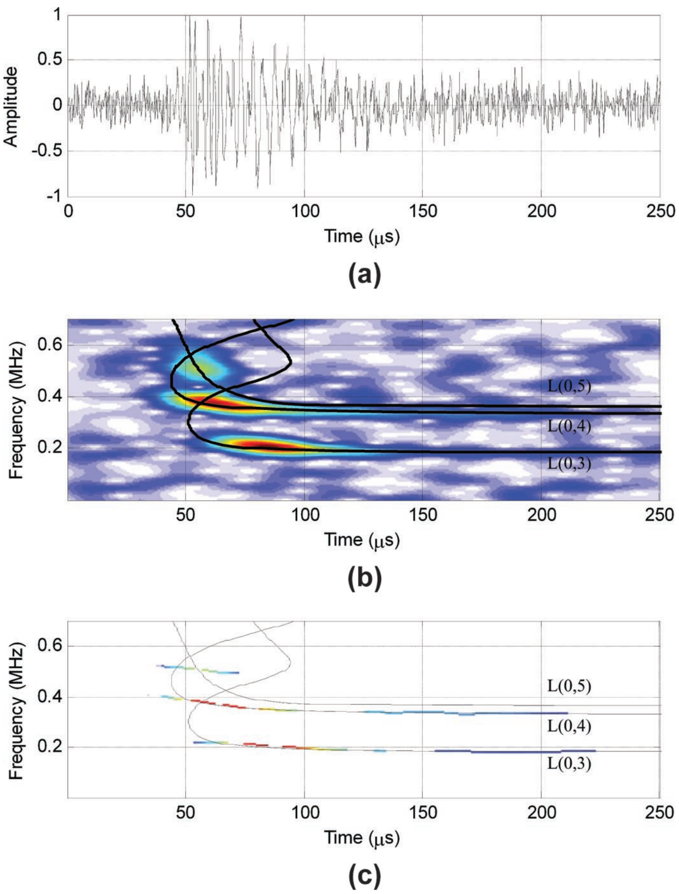

Fig. 5. Noise-polluted multimodal simulated signal (SNR = 0 dB), (a) waveform, (b) TFR, and (c) TFR ridges.

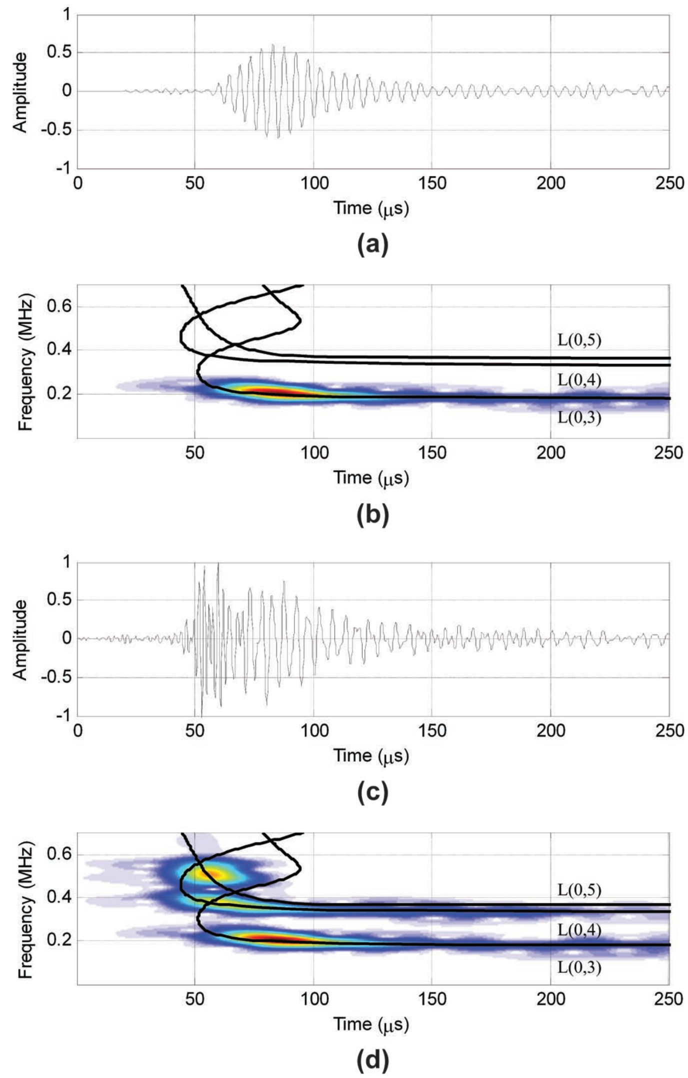

Fig. 6. Separated and reconstructed results of the noise-polluted simulated signal (SNR = 0 dB), (a) waveform and (b) TFR of the separated component L(0,3), (c) waveform, and (d) TFR of the reconstructed multimode signal.

Fig. 7 illustrates the quantitative evaluation results of the noisy simulated signals, where the SNRs vary from 0 dB to ∞ dB (the ∞ dB denotes noise-free). Figs. 7(a), 7(b), and 7(c) are the NRMSEs (%), the SNRs (dB), and correlation coefficients of the separated individual modes (reconstructed from the TFR ridges), respectively. The NRMSE is the root mean square error divided by the range of observed value,

$$\mathrm{NRMSE} = \frac{\sqrt{\left(\sum_{i=1}^{N}[\mathrm{ori}(i) - \mathrm{rec}(i)]^2\right)/N}}{\mathrm{ori}_{\max} - \mathrm{ori}_{\min}}. \quad (8)$$

The value of NRMSE is often expressed as a percentage; lower values indicate less residual variance. All of these indices are obtained by the comparisons between the reconstructed and corresponding noise-free simulated components, whereas the total reconstructed signals, which are the sums of the reconstructed individual modes, are compared with the noise-free multimodal signal in Fig. 3(b). The NRMSEs decrease with increasing SNRs, but the poorest ones are less than 3.92%. The errors of the lower-order modes are less than those of the higher-order modes, which illustrates that higher-order modes are easily subjected to noise in this method. The main reason for this is that the frequencies of higher-order modes are greater than those of lower-order modes, and during the reconstruction process, there is an operation equivalent to a kind of interpolation that estimates the remainder using some samples. Therefore, the ridge samples of higher-order modes are relatively rougher than those of lower-order modes. A higher sample ratio can improve the NRMSE of the higher-order modes, but the relative difference between the higher and lower modes will still exist. The varying trends of the reconstructed SNRs, the opposite to those of the NRMSEs, increase with the improvement of the simulated SNRs [see Fig. 7(b)]. Even under the worst condition, where the signal and noise have equal variance (SNR = 0 dB), the SNR of the total reconstructed signal can be retained at 10.31 dB, and the SNR of the reconstructed L(0,5) is about 4.67 dB. Fig. 7(c) shows the results of the correlation coefficients. The correlation coefficients of the total reconstructed signals are higher than 0.95 and their average is 0.98; the worst correlation coefficients of L(0,5) are higher than 0.85 and average is

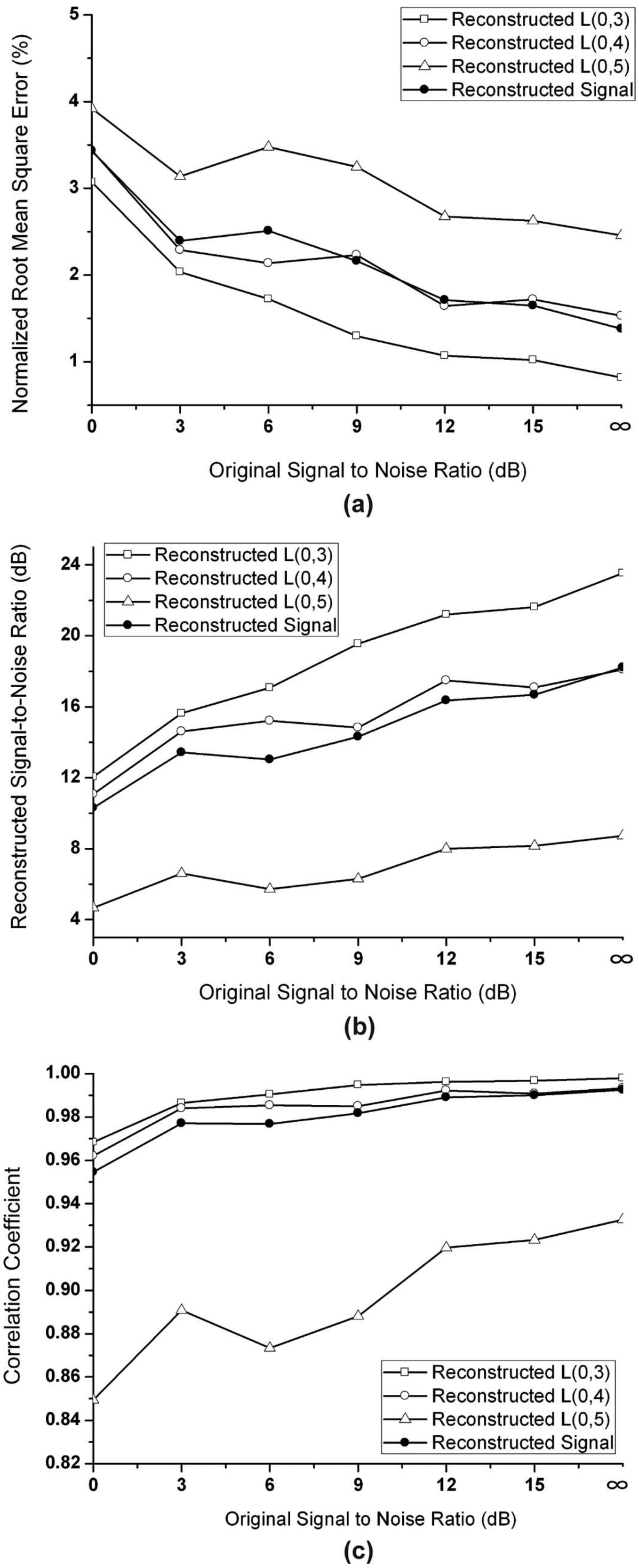

Fig. 7. Separated and reconstructed results of the simulated signals for varying SNRs: (a) NRMSEs (%), (b) SNRs (dB) of the reconstructed signals, and (c) correlation coefficients between the reconstructed and original noise-free simulated signals.

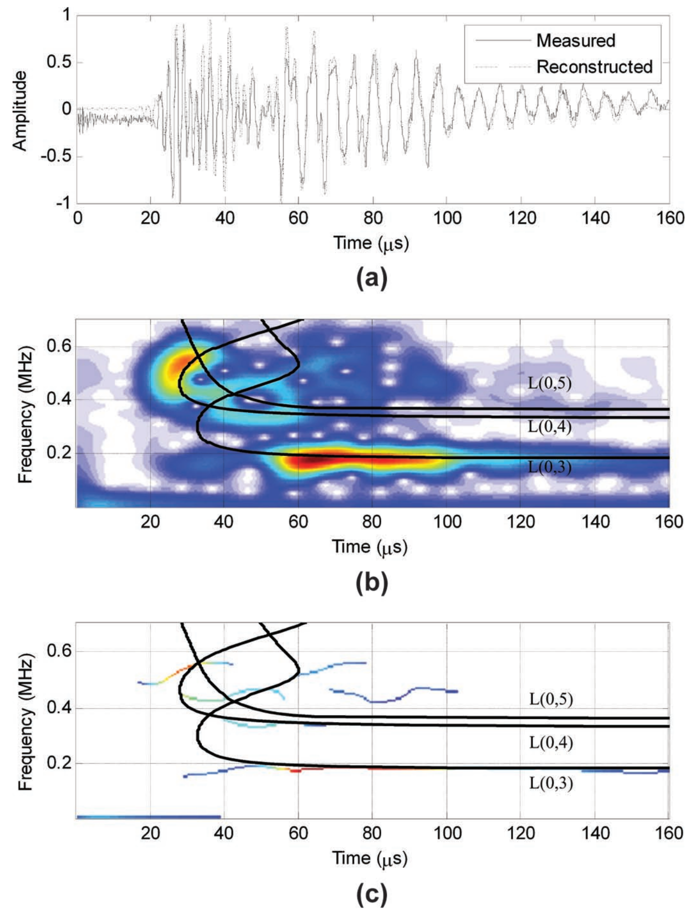

Fig. 8. Analysis of the experimental bovine signal: (a) measured and reconstructed waveforms, (b) TFR, and (c) TFR ridges of the measured waveform.

0.90. These results indicate that the method is robust to the multimodal signals with or without noise and capable of preserving most of the original energy after separation.

C. Experimental Signal

The crazy-climber TFR ridge detection and reconstruction techniques are further demonstrated by experimental signals from bovine tibiae. A 160-μs bovine tibia multimodal signal is shown as an example in Fig. 8(a), and the reconstructed waveform is also plotted for comparison. The consistency between the reconstructed and original signals demonstrates the accuracy of this method, and the smoothness of the reconstruction indicates the de-noising effect and that some baseline drift is also suppressed. Fig. 8(b) shows the TFR of the original signal and three different modes L(0,3), L(0,4), and L(0,5) can be noted. The ridges were detected by 500 climbers, and except for some pseudo-components, these modes are clearly separated in Fig. 8(c). Because each ridge is processed individually in our reconstruction, these noisy components (they might be random noise, scattering, reflection, etc.) can be easily discriminated by their small amplitudes and can be removed by applying some threshold. It is difficult to separate the real individual mode waveforms from the experi-

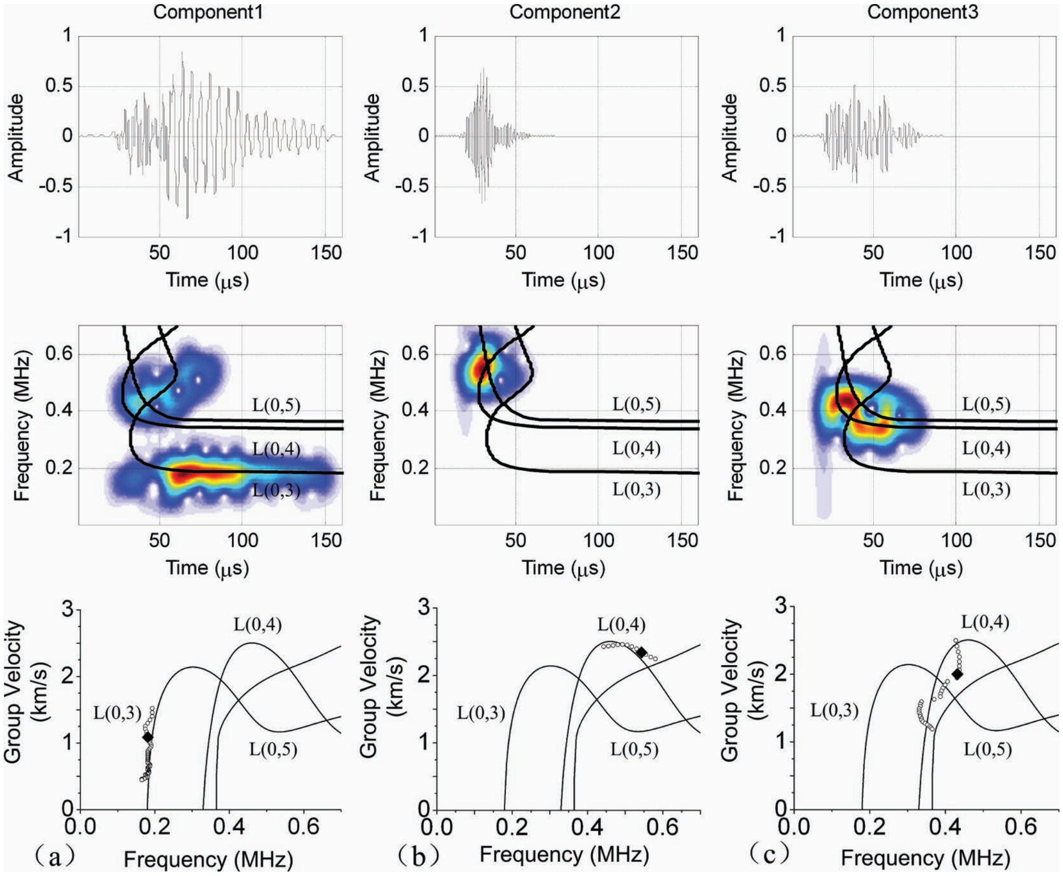

Fig. 9. Separated results of the experimental bovine signal: (a) component 1, (b) component 2, and (c) component 3.

mental signal completely. Thus the TFRs of these three separated individual modes were calculated for comparisons. Because there are three modes in the experimental signal, the components of a single mode were selected and summed together. Fig. 9 illustrates the separated results of the experimental bovine signal; Fig. 9(a), 9(b), and 9(c) show components 1, 2, and 3, respectively. The top plots are the waveforms; the middle and the bottom ones are the corresponding TFRs and the group velocity extracted from the TFRs. It can be seen that the energies of the separated components are close to the theoretical dispersion curves. The small square marks in the bottom figures (group velocity results) represent the maximal energy points of each component, which can be used to estimate the group velocity for each individual mode. The extracted group velocity points are in agreement with the theoretical dispersion curves, and the average root mean square errors of the group velocity results of component 1, 2, 3 are about 1.02% for theoretical L(0,3), 7.03% for L(0,4), and 16.49% for L(0,4), respectively, which illustrates the successful separation of different modes. However, there are still some limitations to this method. It is difficult to determine whether it is a individual mode of L(0,4) or a mixture of L(0,4) and L(0,5), as shown in Fig. 8(b) and Fig. 9(b). This limitation is due to the inherent properties of the waveguide and the time-frequency resolution limitation. Improvement may be made by exciting the signals using low-frequency transducers, because there are fewer modes at lower frequencies. Additionally, if experimental analysis of wave propagation is provided by varying the acoustical base, more realistic imaging of the existing modes could be obtained. Second, as shown in Fig. 9(a), the mode L(0,3) is separated into two parts, and these different parts may need to be distinguished by manual interaction rather than complete computer separation.

The proposed technique for individual modes separation offers several advantages, not only for ultrasonic guided waves in the long bone, but also for all waveguide studies, such as inspection of metal plates and pipelines in industrial NDE. First, the individual modes can be separated in the time domain, whereas most of the existing contributions were limited to the time-frequency domain. Second, the crazy-climber method is capable of directly measuring the group velocity or finding the TFR ridges, which can be used to reconstruct the original signals. It was also shown that these TFR ridges can be used to make a more accurate comparison between the TFR of the real multimodal signal and the theoretical prediction than using TFR alone. Third, in terms of application, it is convenient to separate individual modes from only one remote obtained signal rather than from a group of shift signals. The information of the individual modes can thus be more rationally obtained than by the shifting method, which requires a uniform bone section assumption. Fourth, this technique is based on a blind separation which can be relatively easy applied. Finally, after obtaining the time-domain individual mode components from a complicated multimodal signal, the waveguide information, such as energy ratio, velocity, amplitude, coefficients of attenuation, transmission, and reflection can be independently and precisely computed.

V. Conclusions

A time-frequency-based modes separation technique was presented to analyze ultrasonic guide waves in long cortical bones. For the simulated signals with or without noise, the individual modes can be reconstructed from corresponding ridges. Meanwhile, it was shown that these methods are also robust with the bovine tibia experimental signal. The main advantage is that this method can separate the TFR ridges and reconstruct the corresponding time-domain individual components without any *a priori* knowledge. Furthermore, it allows for efficient comparisons between the obtained TFR ridges and the theoretical dispersion curves, and quantitative estimation of propagation parameters for each mode individually. They both are essentially useful for inverse assessment of bone properties from ultrasonic signals.

However, from a point of application, it is still difficult to determine the modal energy attribution at some time-frequency areas because of time-frequency uncertainty. Improvements may be made by acquiring fewer mode signals by using low-frequency transducers. Additionally, the identification of different modes still needs to be performed by manual interaction, rather than automatic computer separation. Finally, this paper did not provide detailed discussion of the mode characteristics varied with the overlying soft tissues, and cortical thickness, which must be investigated in further studies.

In conclusion, the methods presented provide a powerful signal processing tool for analyzing multimodal ultrasonic axial transmission signals in long bones, regardless of the specific setup used. In particular, ability of the methods to extract quantitative data for experimental *in vitro* signals was demonstrated. Detailed evaluation of the feasibility of the methods on different measurement setups and bone samples still provides challenges for further studies. Moreover, these methods may also prove useful for other applications of NDE.

References

[1] P. Laugier, M. Talmant, and T. L. Pham, "Quo vadis, ultrasonics of bone? Present state and future trends," *Arch. Acoust.*, vol. 33, no. 4, pp. 553–564, 2008.

[2] M. Talmant, S. Kolta, C. Roux, D. Haguenauer, I. Vedel, B. Cassou, E. Bossy, and P. Laugier, "*In vivo* performance evaluation of bi-directional ultrasonic axial transmission for cortical bone assessment," *Ultrasound Med. Biol.*, vol. 35, no. 6, pp. 912–919, 2009.

[3] K. A. Wear, "Ultrasonic scattering from cancellous bone: A review," *IEEE Trans. Ultrason. Ferroelectr. Freq. Control*, vol. 55, no. 7, pp. 1432–1441, 2008.

[4] K. A. Wear and G. R. Harris, "Frequency dependence of backscatter from thin, oblique, finite-length cylinders measured with a focused transducer—With applications in cancellous bone," *J. Acoust. Soc. Am.*, vol. 124, no. 5, pp. 3309–3314, 2008.

[5] P. Laugier, "Quantitative ultrasound of bone: Looking ahead," *Joint Bone Spine*, vol. 73, no. 2, pp. 125–128, 2006.

[6] H. H. Bolotin and H. Sievanen "Inaccuracies inherent in dual-energy X-ray absorptiometry *in vivo* bone mineral density can seriously mislead diagnostic/prognostic interpretations of patient-specific bone fragility," *J. Bone Miner. Res.*, vol. 16, no. 5, pp. 799–805, 2001.

[7] K. L. Stone, D. G. Seeley, L. Lui, J. A. Cauley, K. Ensrud, W. S. Browner, M. C. Nevitt, and S. R. Cummings, "BMD at multiple sites and risk of fracture of multiple types: Long-term results from the study of osteoporotic fractures," *J. Bone Miner. Res.*, vol. 18, no. 11, pp. 1947–1954, 2003.

[8] P. Moilanen, "Ultrasonic guided waves in bone," *IEEE Trans. Ultrason. Ferroelectr. Freq. Control*, vol. 55, no. 6, pp. 1277–1286, 2008.

[9] C. C. Glüer, "Quantitative ultrasound—It is time to focus research efforts," *Bone*, vol. 40, no. 1, pp. 9–13, 2007.

[10] V. C. Protopappas, M. G. Vavva, D. I. Fotiadis, and K. N. Malizos, "Ultrasonic monitoring of bone healing," *IEEE Trans. Ultrason. Ferroelectr. Freq. Control*, vol. 55, no. 6, pp. 1243–1255, 2008.

[11] D. A. Ta, K. Huang, W. Q. Wang, Y. Y. Wang, and L. H. Le, "Identification and analysis of multimode guided waves in tibia cortical bone," *Ultrasonics*, vol. 44, suppl. 1, pp. e279–e284, 2006.

[12] V. C. Protopappas, D. I. Fotiadis, and K. N. Malizos, "Guided ultrasound wave propagation in intact and healing long bones," *Ultrasound Med. Biol.*, vol. 32, no. 5, pp. 693–708, 2006.

[13] V. C. Protopappas, I. C. Kourtis, L. C. Kourtis, K. N. Malizos, C. V. Massalas, and D. I. Fotiadis, "Three-dimensional finite element modeling of guided ultrasound wave propagation in intact and healing long bones," *J. Acoust. Soc. Am.*, vol. 121, no. 6, pp. 3907–3921, 2007.

[14] D. Ta, W. Wang, Y. Wang, L. H. Le, and Y. Zhou, "Measurement of the dispersion and attenuation of cylindrical ultrasonic guided waves in long bone," *Ultrasound Med. Biol.*, vol. 35, no. 4, pp. 641–652, 2009.

[15] K. Xu, D. Ta, W. Wang, and P. Moilanen, "Simulation of propagation characteristics of ultrasonic guided waves in the fractured long bone," in *IEEE Int. Ultrasonics Symp. Proc.*, 2008, pp. 233–236.

[16] J. Li and J. L. Rose, "Implementing guided wave mode control by use of a phased transducer array," *IEEE Trans. Ultrason. Ferroelectr. Freq. Control*, vol. 48, no. 3, pp. 761–768, 2001.

[17] Y. Y. Kim, C. I. Park, S. H. Cho, and S. W. Han, "Torsional wave experiments with a new magnetostrictive transducer configuration," *J. Acoust. Soc. Am.*, vol. 117, no. 6, pp. 3459–3468, 2005.

[18] D. Alleyne and P. Cawley, "A two-dimensional Fourier transform method for the measurement of propagating multimode signals," *J. Acoust. Soc. Am.*, vol. 89, no. 3, pp. 1159–1168, 1991.

[19] P. Moilanen, P. H. Nicholson, V. Kilappa, S. Cheng, and J. Timonen, "Measuring guided waves in long bones: Modeling and experiments in free and immersed plates," *Ultrasound Med. Biol.*, vol. 32, no. 5, pp. 709–719, 2006.

[20] M. Niethammer, L. J. Jacobs, J. Qu, and J. Jarzynski, "Time-frequency representations of Lamb waves," *J. Acoust. Soc. Am.*, vol. 109, no. 5, pt. 1, pp. 1841–1847, 2001.

[21] N. E. Huang, Z. Shen, S. R. Long, M. C. Wu, H. H. Shih, Q. Zheng, N. Yen, C. C. Tung, and H. H. Liu, "The empirical mode decomposition and Hilbert spectrum for nonlinear and non-stationary time series analysis," *Proc. R. Soc. Lond. A*, vol. 454, no. 1971, pp. 903–995, 1998.

[22] C. Luo, D. Ta, W. Li, and W. Wang, "Analysis of ultrasonic guided waves in long bones and cortical thickness based on time-frequency methods," *Chin. J. Acoust.*, vol. 34, no. 5, pp. 416–422, 2009.

[23] M. Sasso, G. Haiat, M. Talmant, P. Laugier, and S. Naili, "SVD-based algorithm for axial transmission ultrasound technique application to cortical bone characterization," *IEEE Trans. Ultrason. Ferroelectr. Freq. Control*, vol. 55, no. 6, pp. 1328–1332, 2008.

[24] M. Sasso, M. Talmant, G. Haiat, S. Naili, and P. Laugier, "Analysis of the most energetic late arrival in axially transmitted signals in cortical bone," *IEEE Trans. Ultrason. Ferroelectr. Freq. Control*, vol. 56, no. 11, pp. 2463–2470, 2009.

[25] J. G. Minonzio, M. Talmant, and P. Laugier, "Measurement of guided mode phase velocities using multi-emitters and multi-receivers arrays in contact and transmission matrix analysis: Application to cortical bone evaluation," in *Proc. IEEE Int. Ultrasonics Symp.*, Sep. 20–23, 2009, pp. 1–4.

[26] W. H. Prosser, M. D. Seale, and B. T. Smith, "Time-frequency analysis of the dispersion of Lamb modes," *J. Acoust. Soc. Am.*, vol. 105, no. 5, pp. 2669–2676, 1999.
[27] H. Kuttig, M. Niethammer, S. Hurlebaus, and L. J. Jacobs, "Model-based analysis of dispersion curves using chirplets," *J. Acoust. Soc. Am.*, vol. 119, no. 4, pp. 2122–2130, 2006.
[28] O. Kotte, M. Niethammer, and L. J. Jacobs, "Lamb wave characterization by differential reassignment and non-linear anisotropic diffusion," *NDT Int.*, vol. 39, no. 2, pp. 96–105, 2006.
[29] R. A. Carmona, W. L. Hwang, and B. Torrésani, "Multiridge detection and time-frequency reconstruction," *IEEE Trans. Signal Process.*, vol. 47, no. 2, pp. 480–492, 1999.
[30] L. De Marchi, A. Marzani, S. Caporale, and N. Speciale, "Ultrasonic guided-waves characterization with warped frequency transforms," *IEEE Trans. Ultrason. Ferroelectr. Freq. Control*, vol. 56, no. 10, pp. 2232–2240, 2009.
[31] L. De Marchi, K. Xu, D. Ta, A. Marzani, S. Caporale, and N. Speciale, "Warped signal dictionaries for the analysis of ultrasonic guided waves in long bones," *Proc. IEEE Int. Ultrasonics Symp.*, Sep. 20–23, 2009, pp. 1930–1933.
[32] L. Cohen, "Time-frequency distributions—A review," *Proc. IEEE*, vol. 77, pp. 941–981, 1989.
[33] I. Daubechies, "The wavelet transform, time-frequency localization, and signal analysis," *IEEE Trans. Inf. Theory*, vol. 36, no. 5, pp. 961–1005, 1990.
[34] R. J. McAulay and T. F. Quatieri, "Speech analysis/synthesis based on a sinusoidal representation," *IEEE Trans. Acoust. Speech Signal Process.*, vol. ASSP-34, no. 4, pp. 744–754, 1986.
[35] P. Flandrin and P. Goncalves, "Geometry of affine time-frequency distributions," *Appl. Comput. Harmon. Anal.*, vol. 3, no. 1, pp. 10–39, 1996.
[36] W. R. Gilks, S. Richardson, and D. J. Spiegelhalter, Eds. *Markov Chain Monte Carlo in Practice*, London, UK: Chapman & Hall, 1995.
[37] L. Elvira-Segura, "Acoustic wave dispersion in a cylindrical elastic tube filled with a viscous liquid," *Ultrasonics*, vol. 37, no. 8, pp. 537–547, 2000.
[38] P. D. Wilcox, "A rapid signal processing technique to remove the effect of dispersion from guided wave signals," *IEEE Trans. Ultrason. Ferroelectr. Freq. Control*, vol. 50, no. 4, pp. 419–427, 2003.
[39] H. Jansons, A. Tatarinov, V. Dzenis, and A. Kregers, "Constructional peculiarities of the human tibia defined by reference to ultrasound measurement data," *Biomaterials*, vol. 5, no. 4, pp. 221–226, 1984.
[40] F. Lefebvre, Y. Deblock, P. Campistron, D. Ahite, and J. J. Fabre, "Development of a new ultrasonic technique for bone and biomaterials in vitro characterization," *J. Biomed. Mater. Res.*, vol. 63, no. 4, pp. 441–446, 2002.
[41] P. Moilanen, P. H. Nicholson, V. Kilappa, S. Cheng, and J. Timonen, "Assessment of the cortical bone thickness using ultrasonic guided waves: Modelling and in vitro study," *Ultrasound Med. Biol.*, vol. 33, no. 2, pp. 254–262, 2007.

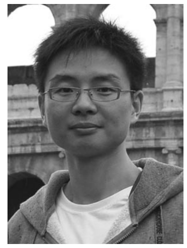

Kailiang Xu was born in Zhejiang, China, in 1985. He received the dual B.S. degrees in electronic information science and technology and computer science from Inner Mongolia University, China, in 2006. He is currently a Ph.D. student at the Department of Electronic Engineering in Fudan University. His main research fields of interest are biomedical ultrasound, guided wave signal processing, and boundary element method simulation of long bone.

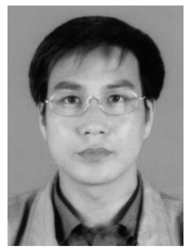

Dean Ta was born in China in October, 1972. He received M.S. and Ph.D degrees from the Institute of Acoustics in Shaanxi Normal University and Tongji University, China in 1999 and 2002, respectively. He was a Postdoctoral researcher at the Department of Electronic Engineering, Fudan University, from 2002 to 2004. Now, he is a professor at Fudan University. His research interests include biomedical ultrasound, medical signal processing, diagnosis system of medical ultrasound; the generation, propagation and applications of ultrasonic guided waves in medicine; and NDE & E. He has published about 80 papers.

Weiqi Wang was born in Shanghai, China on May, 1939. He graduated from the Physics Department of Fudan University in 1961. He was elected to be a member of the Chinese Academy of Engineering in 1999. He is the executive professor and supervisor of the Ph.D. program in Fudan University. He was the recipient of an AIUM/WFUMB Pioneer Award, a National Invention Award (2nd place), and other 17 awards. His research interests involve some areas of ultrasound and electronics, including signal analysis, processing, and ultrasound imaging. He is the director of several academic associates, such as the Chinese Associate of Acoustics.